PROCEEDINGS, 51st Workshop on Geothermal Reservoir Engineering
Stanford University, Stanford, California, February 9-11, 2026
SGP-TR-230

Modeling Thermal Evolution: A Lifecycle Approach to Temperature Gradients of Enhanced Geothermal Systems

Lijun Song, Mark Milkovisch, Rafael Rodriguez Romo, Mehdi Hizem

SLB, 555 Industrial Blvd, Sugar Land TX 77478

Keywords: Enhanced Geothermal, Tempering, CFD

ABSTRACT

This study investigates the thermal behavior of an Enhanced Geothermal System (EGS) well during production and wireline intervention, with emphasis on how wellbore heating influences the feasibility and safety of wireline operations. A major challenge is maintaining surface temperatures within limits to ensure compatibility with Pressure Control Equipment (PCE) and wireline systems under high-temperature conditions.

A thermal model was developed using real temperature data from Utah 16B(78)-32 well up to 6,000 ft, supplemented by two artificial high-temperature scenarios (bottom-hole temperatures of 250 °C and 300 °C) for depths between 6,000 and 18,000 ft. The axisymmetric model incorporates heat transfer through fluid convection and solid conduction in both axial and radial directions. The simulation consisted of five phases: establishing initial conditions with real and artificial temperature profiles; production at 2,000 gal/min; a one-hour shut-in; tempering with 400 gal/min of 25 °C water for two hours; and a 24-hour wireline operation period, during which surface temperature was targeted to remain below 80 °C to prevent flashing and steam formation with a 20 °C margin.

Results reveal significant heat retention in the formation during production, leading to reheating during wireline operations despite prior tempering. For the 250 °C case, proper tempering maintained surface temperatures below 80 °C for 24 hours, enabling safe wireline or coiled tubing work. In contrast, for the 300 °C case, surface temperature rose to 86.2 °C after 24 hours, slightly exceeding the limit.

This work underscores the importance of surface temperature control and highlights the need for practical thermal management strategies to ensure safe and efficient geothermal wireline operations. The developed model serves as a predictive tool for assessing thermal behavior under various operational scenarios, supporting proactive planning and minimizing intervention downtime.

1. INTRODUCTION

Geothermal energy is a clean and renewable power source derived from the Earth's internal heat. This sustainable thermal energy can be used directly for heating in residential and industrial applications or indirectly for electricity generation. It plays a vital role in reducing greenhouse gas emissions and diversifying energy portfolios, especially in regions with favorable geological conditions (Elshehabi and Alfehaid, 2025, Kabeyi 2019). The United States possesses a tremendous number of geothermal resources, offering valuable opportunities for both domestic and commercial utilization.

Enhanced Geothermal Systems (EGS) is a promising method to extract heat from hot, dry rock formations, which significantly broadens the geographical scope for geothermal energy development (Ziagos et al., 2013, Hamm et al., 2021; Kumar et al., 2022; Moya et al., 2018). Particularly, the Utah Frontier Observatory for Research in Geothermal Energy (FORGE) is a Department of Energy (DOE)-funded project tasked with addressing various challenges associated with EGS, such as high drilling costs, inefficiencies in heat extraction, and minimizing the environmental impacts of geothermal energy development (Dupriest and Noynaert, 2024; Lellouch et al., 2020).

While the conventional geothermal systems that rely on naturally existing reservoirs of hot water or steam, EGS can be deployed in areas where such resources do not exist on the ground level. First, an injection well is established into the underground region where the rock formations are sufficiently hot at depth. Then, high pressure water is pumped through the injection well to the hot rock formation creating fractures and forming a network of pathways. As the water moves through these pathways, it absorbs thermal energy from the surrounding rock. The heated water is then pumped back to the ground surface through a production well. In both wells, steel casing is deployed to maintain the structural integrity of the well to ensure safe and efficient operation. These wells are drilled to significant depths, often several kilometers, where the surrounding rock formations can be unstable and subject to high temperatures and pressures. Casing provides a barrier that stabilizes the well and isolates different geological layers, protecting freshwater aquifers near the surface and confining geothermal fluids within the designed system. As EGS wells operate under extreme conditions, casing failure could result in wellbore collapse, and/or cement integrity could be damaged causing fluid losses and thermal transmission inefficiencies. These could cause environmental and operational issues.

A critical element of geothermal applications is wireline survey technology (Martuganova et al., 2022; Susan et al., 2024) which plays an essential role in characterizing subsurface conditions and monitoring reservoir behavior during stimulation and production which cannot be obtained from surface observations alone. Wireline tools provide accurate in situ measurements of casing conditions, temperature, pressure, rock properties, and fluid flow within boreholes, delivering the data needed to optimize reservoir development and maintain safe, effective operations. These measurements enable engineers to understand reservoir dynamics, ensure proper construction and

operation, and make informed decisions about well performance and long-term monitoring. The integration of advanced geothermal energy concepts with sophisticated wireline measurement techniques positions the Utah FORGE project at the forefront of geothermal research.

Wireline surveys involve lowering instruments into a well on a cable to collect important data about what's happening deep underground. In geothermal projects, these tools face extremely high temperatures - often between 200 and 300°C. High heat can damage seals and cables, so the entire tool must be built to withstand these harsh conditions for reliable and safe operation . If the heat exceeds the limits of the tool's electronics or batteries, the equipment can fail, leading to wrong readings or complete breakdown. To control the temperature and heat, wireline tools are designed with special heat-resistant components, insulation, and cooling systems. Pressure Control Equipment (PCE) is installed at the wellhead to safely manage high-pressure fluids during wireline tool deployment.

EGS presents greater safety challenges than conventional wells for wireline operations because of extreme temperatures both downhole and at the surface. For personnel, the primary hazard is the risk of injury during rig-up of PCE on a hot wellhead. The PCE must be rated for high-temperature conditions. The most critical components are non-metallic parts, such as O-rings and grease seals, which must maintain sealing integrity at the required temperature limits. High-temperature-resistant seals, capable of withstanding up to 150 °C, are available but require careful inspection and proper implementation in the tool. In contrast, surface pressures in EGS wells are typically below 1,000 psi which is significantly lower than the 5,000 psi rating commonly used for oil and gas applications. For equipment, in addition to exposure to high downhole temperatures, there is the risk of exceeding the maximum allowable temperature gradient for downhole tools, which are typically limited to less than 0.2 °C/s. For the well itself, there is a potential hazard of cement bond failure, either between the casing and the cement or between the cement and the formation. Typically, a Blowout Preventer (BOP) mounted on the wellhead to seal the well in case of unexpected pressure surges and prevent uncontrolled fluid flow or blowouts (Chaerudin et al., 2021). These systems allow the tool to be inserted without fully depressurizing the well, maintaining the pressure so that the fluid remains in liquid phase.

Managing and conditioning well temperature is critical before opening the wellhead for wireline tool deployment. This process typically involves a controlled shutdown and tempering sequence. First, production flow is halted by closing the wellhead valves. Next, the well is allowed to cool naturally. This is followed by tempering, achieved by injecting cool water into the well. Controlled tempering is essential to prevent thermal shock, which could damage the casing or compromise cement integrity. The injection process is carefully regulated to ensure a gradual temperature reduction. Once the well has cooled sufficiently, the final phase of operation is shutting down the injection flow, leaving the well for wireline operation.

Predicting wellbore fluid temperatures is critical for planning and executing these processes. The well shall always remain stable and unexpected reheating that could affect subsequent operations should be avoided. Production shutdown, tempering, injection and shutdown involve significant temperature changes in space and time. As soon as production stops, heat flux from the surrounding formation begins to redistribute. Without accurate temperature forecasts, well integrity and safety could be compromised due to thermal stress in the casing and cement. During tempering, the optimal volume and rate of cool water injection need to be determined to achieve the desired temperature within a specific timeframe while preventing thermal shock. Modeling and simulation help extract data needed to optimize operational steps, minimize risks, and maintain well integrity under extreme geothermal conditions. In this study, Computational Fluid Dynamics (CFD) is applied to capture the complex heat exchange between injected fluids, wellbore geometry, and the surrounding rock under extreme temperature and pressure conditions. The wellbore and reservoir are discretized into a computational grid, and the governing conservation equations for mass, momentum, and energy are solved using numerical algorithms. This approach enables the simulation and prediction of fluid temperature profiles during key operations such as production shutdown, tempering, and injection shutdown.

2. WELL GEOMETRY AND TEMPERATURE PROFILE

In this study, a simplified representation of the well geometry and temperature profile is derived from the Utah FORGE production well 16B(78)-32 (Alumbaugh et al., 2025; Utah FORGE, 2023). The simulated well consists of a true vertical section of approximately 8,300 ft and an extended horizontal section of about 10,000 ft. From the surface down to a depth of 6,760 ft, the formation is composed of alluvial sediments, transitioning into a granitoid formation below that depth. The well is completed with multiple casing strings, including a 7-inch liner within the wellbore and a 20-inch conductor casing at the surface. The complete casing program, along with cementing details and formation characteristics, is illustrated in Figure 1. Notably, a closed water column occupies the annular space between the 7-inch liner and the 13-3/8-inch liner, while cement fills the remaining annuli between other casing strings. The casing, liner, water column, cement dimensions are listed in Table 1.

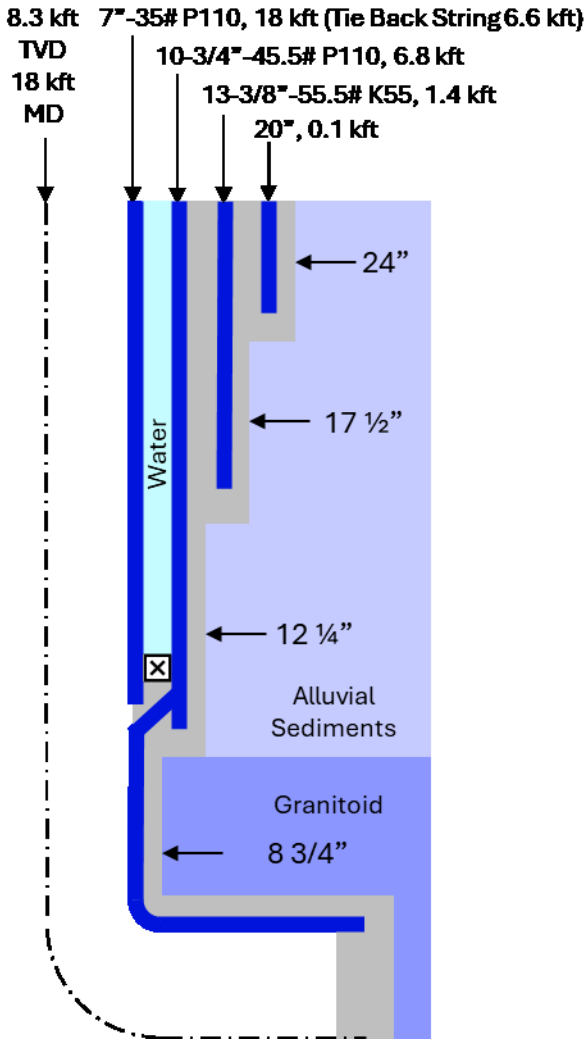

Figure 1: Well, Casing and Formation Geometry

Table 1: Dimensions of Diameter and Length for the Components

Pipe, Cement and Water Sections	OD (in)	ID (in)	Length (ft)
20-inch Conductor	20	19.12	100
13-3/8-inch Surface casing	13.325	12.615	1400
10-3/4-inch Production casing	10.75	9.95	6750
7-inch Tie back string	7	6.004	8300
7-inch Production liner horizontal	7	6.004	10000
Conductor Cement	24	17.5	105
Surface Casing Cement	17.5	12.25	1410
Production Casing Cement	12.25	10.75	6760
Production liner water	9.95	7	6760

3. MODELING AND SIMULATION METHOD

A two-dimensional (2D) Well Flow Temperature Code (WFTC) was developed in a mathematical programming language to simulate thermal behavior in an axisymmetric wellbore configuration. Fluid flow within the wellbore is represented by an average velocity, and

convective heat exchange between the fluid and surrounding solid is evaluated using the established correlations for forced convection. The governing energy equations are discretized and solved iteratively using the Gauss–Seidel method (Saad, Y., 2003) to ensure numerical stability and convergence. The framework incorporates both transient and steady-state formulations, enabling analysis of time-dependent heat transfer as well as equilibrium conditions. for heat transfer in the solid. Equation 1 for the transient 2D axial and radial heat conduction (Incropera et al., 2011) is discretized in an implicit form based on a Finite Volume Method (FVM). Equation 2 of fluid heat conduction is discretized using a discretized in an implicit, upwind scheme based on the Finite Volume method. In Eq. 1 and 2, *r* is the radius, *z* is the axial distance along the well, u is the fluid velocity, *Cp* is the heat capacity, h is the convection coefficient between the fluid and the casing wall. The computational domain employs a structured grid with uniform discretization along the axial direction, while radial cell spacing is stretched to capture near-wall gradients effectively. Boundary conditions are prescribed such that a constant temperature with predetermined thermal resistance or larger formation volume is maintained at the outer formation boundary in the radial direction, located at a diameter of 200 inches, whereas the top and bottom surfaces are treated as adiabatic surfaces.

$$\frac{\partial \rho c_p T}{\partial t} = k\left(\frac{1}{r}\frac{\partial}{\partial r}\left(r\frac{\partial T}{\partial r}\right) + \frac{\partial^2 T}{\partial z^2}\right) \tag{1}$$

$$\frac{\rho c_p \partial T}{\partial t} + u\frac{\rho c_p \partial T}{\partial z} = -\frac{4h}{D}(T - T_w) + k\frac{\partial^2 T}{\partial z^2} \tag{2}$$

During injection and production, forced convective heat transfer between the wellbore fluid and the casing wall was calculated using Correlation 1, as shown in Table 2 (Colburn, 1933), which provides a reliable relationship between the Nusselt number, Reynolds number, and Prandtl number (*Nu, Re, Pr*) for turbulent flow conditions. This correlation accounts for the combined effects of fluid properties and flow regime, making it suitable for high-Reynolds-number flows typically encountered in geothermal wells.

When production or injection flow stops in the vertical section both the annular fluid between the casings and the fluid inside the production casing, heat transfer in the axial direction along the well depth within the fluid is represented by an equivalent velocity calculated such that it produces the same convective heat transfer coefficient as predicted by the Colburn correlation. The heat transfer in the radial direction is evaluated using the Correlation 2 shown in Table 2 (Fouad and Ibl, 1960) where Ra_L is evaluated based on the fluid volumetric expansion coefficient, the fluid temperature difference between the top surface and bottom, and the length of the vertical section. When production or injection flow stops in the horizontal section, natural convection is evaluated using an empirical Correlation 3 shown in Table 2, where the Nusselt number is based on the internal diameter of the liner. This correlation was derived from numerical simulations of heat transfer between the surrounding formation and stagnant water within the horizontal section.

Table 2: Empirical Correlations for Forced and Natural Convection

Index	Empirical Correlation	Area of Application	Main Input Parameters
1	$Nu = 0.023Re^{4/5}Pr^{1/3}$	Forced convection between fluid and casing	Flow velocity
2	$Nu_L = 0.31Ra_L^{0.28}$	Natural convection for fluid within the vertical section	Differential temperature between surface fluid and bottom fluid
3	$Nu_D = 450$	Natural convection in the horizontal section between fluid and casing	Differential temperature between fluid and formation

4. MATERIAL PROPERTIES

Water properties were obtained from NIST REFPROP (Lemmon et al., 2018) at a pressure of 1,450 psi over a temperature range of 20 °C to 300 °C, as illustrated in Figure 3. These properties were implemented locally within the computational grid to account for temperature-dependent variations in density, viscosity, and fluid velocity. For solid materials, the density, heat capacity, and thermal conductivity of Thermalite cement were applied based on specifications of Forterra, 2021 and by Wolterbeek et al., 2013. The thermophysical properties of the surrounding formations—Alluvial Sediment and Granitoid—were adopted from values reported by Gwynn et al., 2019 and Allis et al., 2019. The solid material properties are listed in Table 3.

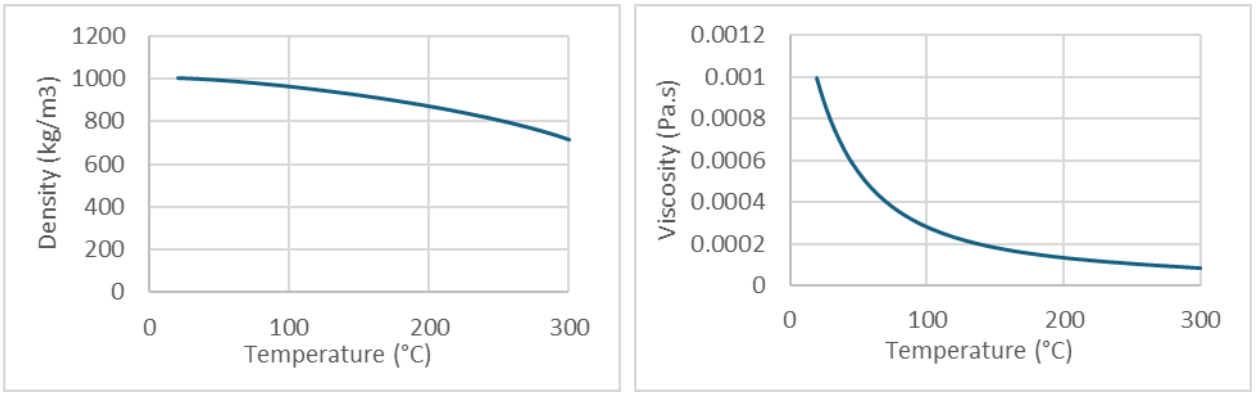

Figure 2: Properties of Water Density and Viscosity at 1450 psi

Table 3: Solid Material Properties

Material	Density, kg/m3	Heat Capacity, J/kg-K	Thermal Conductivity, W/m-K
P110 (casing, liner)	7850	473	42.6
Cement	1900	1400	0.2
Alluvial Sediment	2400	830	2.0
Granitoid	2600	790	3.05

Groundwater at the Utah FORGE site exhibits variable salinity, generally ranging between 4,000 and 6,000 mg/L of total dissolved solids (TDS) (Kirby et al., 2019). To account for salinity effects on water density, an empirical equation proposed by Naftz for Great Salt Lake water was applied, which is valid for temperatures between 5 °C and 50 °C (Naftz, 2011). The resulting density increase due to salinity is approximately proportional to salt concentration and falls within 3 to 6 kg/m³. This adjustment was incorporated into the water density calculation in the current simulation. The influence of salinity on thermal conductivity and heat capacity was assumed to be negligible.

5. MODEL VALIDATION

A series of trial simulations were performed to validate the 2D WTFC code methodology and its implementation. The comparative simulation was conducted using Ansys Fluent (Ansys 2025) which solves the full 2D Navier-Stokes equation in the fluid domain and the heat conduction equation in the solid domain. An axisymmetric geometry was generated and meshed using Ansys Meshing. The mesh is uniform along the axial direction and radially stretches across the fluid, casing, cement, and formation regions. It consists of approximately 0.66 million cells for a numerical injection test case in an 8,300 ft vertical section. The initial temperature profile for both fluid and formation is assumed to be piecewise linear. Injection conditions include a temperature of 50 °C and a flow rate of 340 gal/min. Figure 3 illustrates fluid temperatures along the wellbore at three different time intervals. Results indicate that, under forced convection between the fluid and surrounding casing and formation, the difference between 2D full Navier-Stokes (NS) formulation and the WTFC code predictions is negligible.

Another validation case was performed to assess natural convection in a long vertical well, which also includes an additional 10,000 ft horizontal section. This well geometry is longer than the previous one. The mesh was constructed in Ansys Meshing using the same approach as before. The initial ambient formation and fluid temperatures were derived from the steady-state production profile, with a bottom-hole temperature of 235 °C. Figure 4 presents the computed temperature distribution after 1 hr. of production flow shutdown. The results show that temperature differences between the WFTC code and the 2D NS along the well depth remain within 1 °C after the production flow shut down.

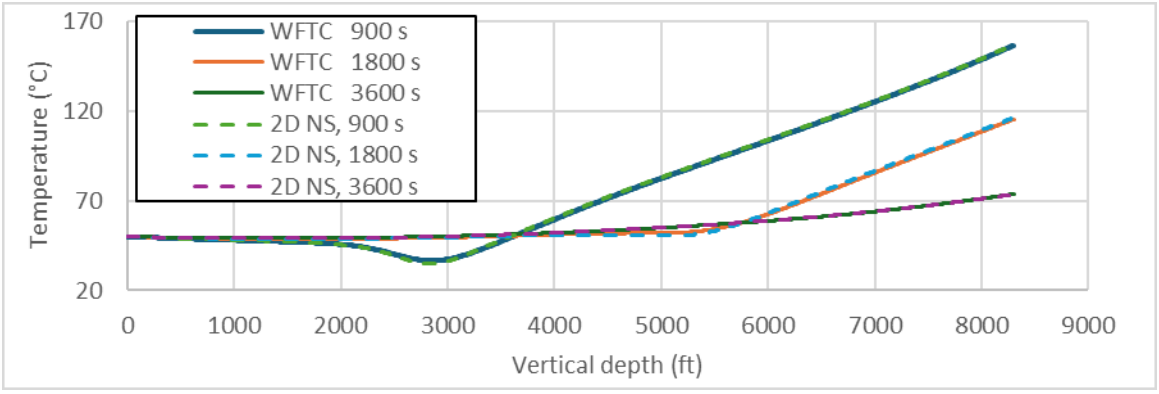

Figure 3: Validation Case 1: WFTC Comparison with Ansys Fluent for Forced Convection in An 8300 ft Vertical Well

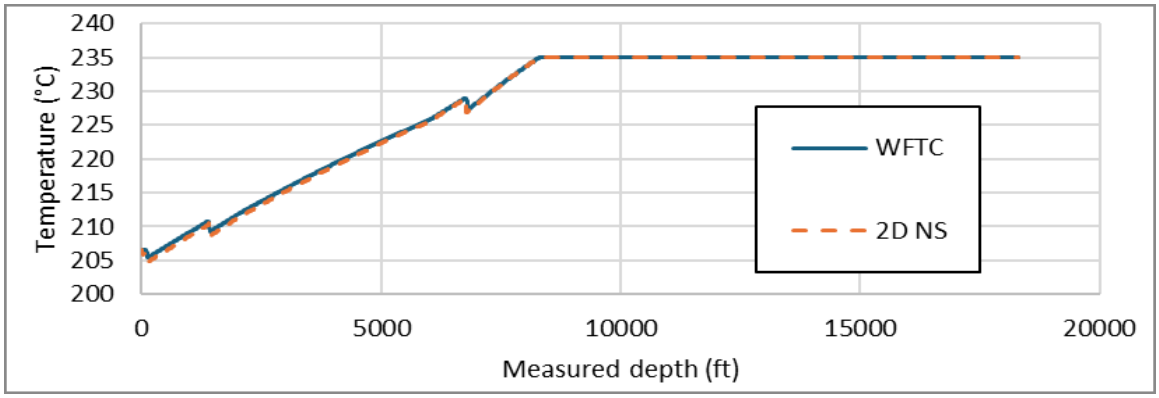

Figure 4: Validation Case 2: WFTC Comparison with Ansys Fluent for Natural Convection in An 8300 ft Vertical and 10000 ft Horizontal Well. Results Are Shown at 1 hr. After Production Flow Shut Down.

Thus, the selected model for both forced and natural convection is validated, with WTFC closely matching results from a full Navier–Stokes formulation. Moreover, WTFC delivers substantially higher computational efficiency: a 24 hr. simulation typically completes in about 10 minutes on a single CPU core, compared to roughly 80 minutes on 20 cores using the 2D full Navier–Stokes approach—an estimated speedup of over 100. In addition, the WTFC code provides greater flexibility by allowing easy modification of material properties and geometric dimensions without the manual meshing and setup typically required in commercial software. This capability simplifies parametric studies and supports design-of-experiment approaches for "what-if" scenarios. Additionally, the code can be integrated into other programs for system-level job evaluation and real-time monitoring.

6. SIMULATED CONDITIONS

Temperature data from well 16B(78)-32 was utilized up to a depth of approximately 6,000 ft. Beyond this depth, two hypothetical high-temperature scenarios were introduced between 6,000 and 8,300 ft. The resulting temperature profile, shown in Fig. 2, begins at 15 °C at the surface, rises to 66 °C at 2,000 ft, and reaches 150 °C at 6,000 ft. At 8,300 ft, two cases were considered: 250 °C and 300 °C. With a total depth of 18,300 ft, the modeled formation extends radially to a diameter of 200 inch, where the ambient formation temperature is applied. This diameter or the thermal resistance at the diameter can be adjusted based on field data of heat dissipation to the surrounding formation.

The solid domain was discretized using a structured mesh with uniform cell spacing along the axial direction and a radially stretched distribution to capture geometric variations. For the wellbore fluid region, the mesh was represented by a single line of nodal points along the axis. In this study, computational mesh comprises approximately 6,100 cells axially and 100 cells radially.

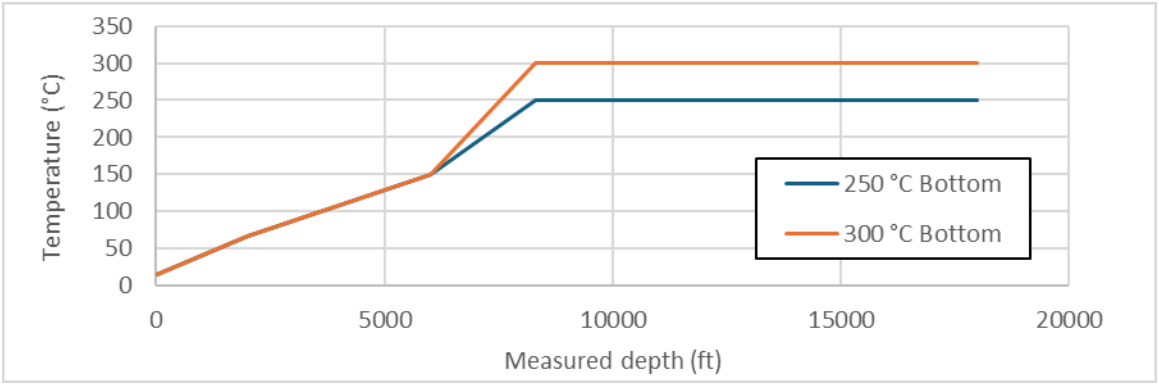

Figure 5: Profile of Ambient Formation Temperature along The Measured Well Depth

The simulation incorporates a sequence of operational phases representative of typical well intervention procedures:

1. ***Production Phase:*** The well is operated at a steady-state production flow rate of 2,000 gal/min, establishing initial temperature conditions within the wellbore and surrounding formation.

2. ***Shut-in Phase:*** Following the shutdown of production, the well remains static for 1 hr. The wellbore fluid , casing and cement naturally cool down during non-flow conditions.

3. ***Tempering Phase***: A controlled tempering operation is initiated by circulating water at 400 gal/min with an inlet temperature of 25 °C for 2 hrs. This step is designed to reduce wellbore temperatures prior to subsequent interventions, mitigating thermal risks to equipment and personnel.

4. ***Wireline Operations:*** A 24 hr. intervention period is simulated. To prevent flashing and steam formation, surface equipment temperatures should be maintained below 80 °C, providing an approximate 20 °C safety margin. This phase reflects operational constraints for safe handling and tool deployment under high-temperature conditions. In this study, while the focus is on the overall wellbore and surface fluid temperature, the movement of the wireline tool itself is not included.

7. SIMULATION RESULTS

For the case with a bottom-hole formation temperature of 250 °C and a steady state production flow rate of 2,000 gal/min, the temperature distribution within the solid domain—including casing, cement, and formation—is shown in Fig. 6. The contour is highly elongated due to the large axial length of 18,300 ft compared to the relatively small formation radius of 100 inch. As expected, the temperature below 8,300 ft remains constant at 250 °C. Moving upward, the temperature at the outer formation radius decreases progressively, following the prescribed ambient temperature profile.

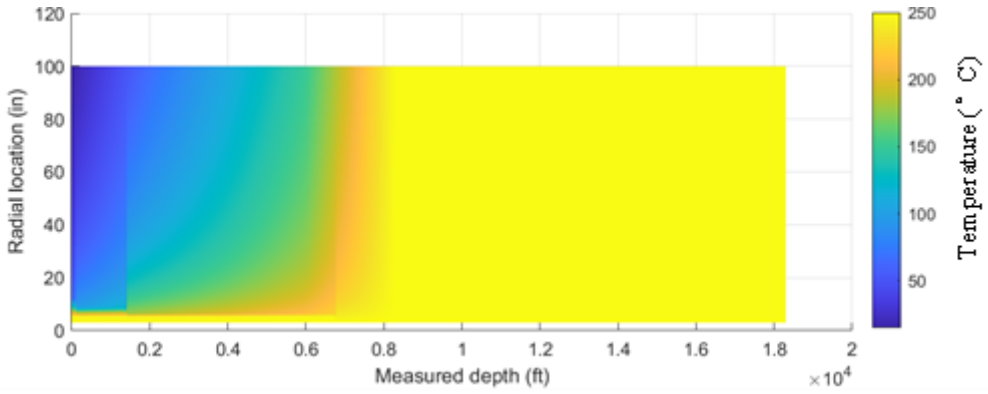

Figure 6: Steady-State Well Temperature for 250 °C Bottom Formation at 2,000 gal/min Production

Figure 7 illustrates the corresponding fluid temperature distribution along the well depth. The average fluid velocity is approximately 22.67 ft/s in the well bore. At this high flow rate, convective transport dominates, and heat loss to the surrounding formation is relatively small. The outlet temperature at the surface is 247.9 °C, representing only a 2.1 °C reduction from the bottom-hole temperature. For the second scenario with a bottom-hole temperature of 300 °C, the surface outlet temperature at the surface is 296.7 °C, corresponding to a 3.3 °C reduction from the bottom-hole temperature.

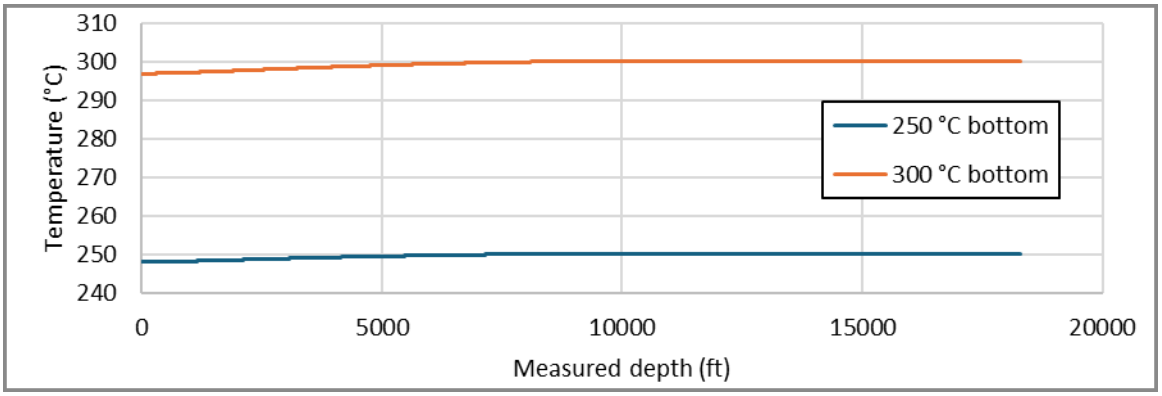

Figure 7: Steady-State Fluid Temperature at 2,000 gal/min Production

After production flow is shut down, the forced convection within the wellbore fluid ceased, and natural convection became the dominant heat transfer mechanism along the axial direction of the fluid and between the casing and the fluid. Figure 8 illustrates the fluid temperature distribution along the well depth 1 hr. after shutdown. For both cases of 250 °C bottom and the 300 °C bottom, in the horizontal section below 8,300 ft, the temperature remains close to that in the bottom of the well. Above 8,300 ft, the temperature gradually decreases with decreasing depth, following the cooler ambient formation conditions. Interestingly, the temperature profiles are not monotonic; instead, they exhibit distinct stepwise variations at locations where the casing and cement configurations change. This behavior primarily results from differences in radial heat loss rates and heat residual associated with varying casing and cement thicknesses.

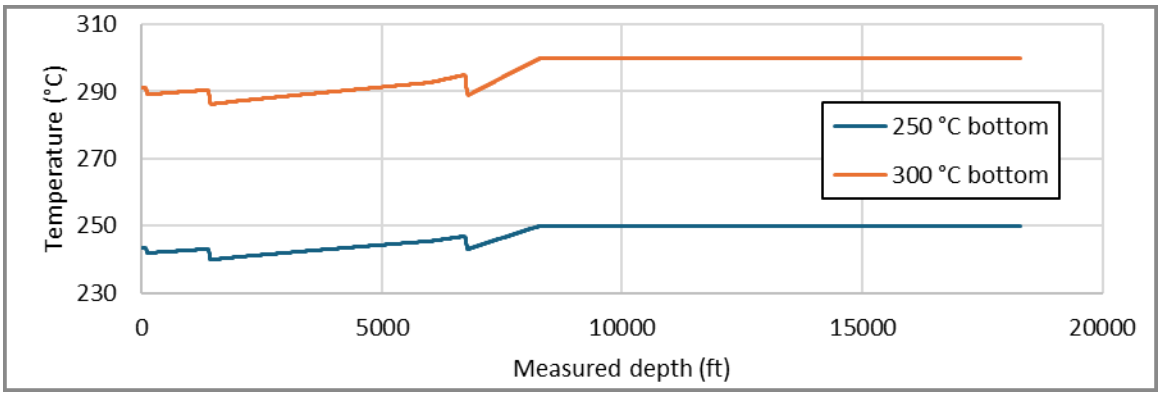

Figure 8: Fluid Temperature at 1 Hr. After Production Shutdown

During the subsequent tempering stage, forced convection resumes with an injection flow rate of 400 gal/min and an inlet fluid temperature of 25 °C. Figure 9 illustrates the transient outflow temperatures at the well bottom throughout this process. Theoretically, it takes about 1.12 hrs. for the injected fresh fluid to fully displace the previous production fluid. Throughout the injection process, the injected fluid gradually heats up while the casing, cement, and surrounding formation cool down. After 2 hrs. of injection, the bottom-hole outflow temperature reaches approximately 214 °C for the 250 °C bottom-hole condition and 252 °C for the 300 °C bottom-hole condition.

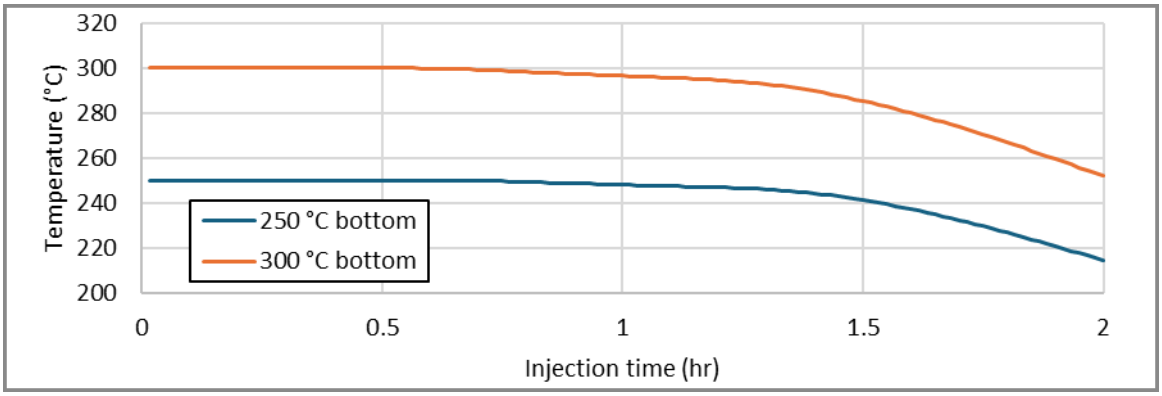

Figure 9: Bottom Fluid Outlet Temperature with 400 gal/min Injection

Figure 10 illustrates the fluid temperature distribution along the well depth after 2 hrs. of injection. In both cases, the injection flow has effectively smoothed the stepwise variations observed in the temperature profiles during the previous shutdown phase. Due to the

temperature difference between the injected fluid and the surrounding formation, the temperature increase rate appears to be higher near the beginning of the horizontal section of the well.

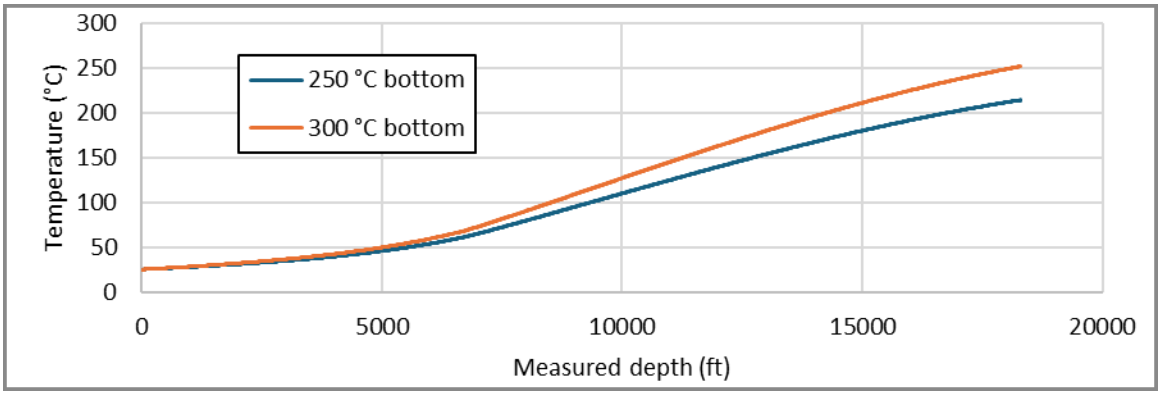

Figure 10: Fluid Temperature Along the Well After 2 Hr. 400 gal/min Injection

During the tempering operation, the production casing experiences the highest temporal temperature gradient of the four phases of operation. Figure 11 presents the local maximum gradient over time at depths within 500 ft. As one can imagine, the largest gradient occurs at the ground surface, where cold fluid is introduced into a hot well, creating a sharp temperature shock. Peak temporal gradients of approximately −80 °C/s are observed at the well entrance for the 250 °C bottom-hole condition, and -64 °C/s for the 300 °C bottom-hole condition. In practical applications, the gradients will likely to be lower due to longer actual ramp-up duration of the injection process. The temporal temperature gradient is related to spatial temperature gradient in the casing and formation. A comprehensive structural analysis will be required to determine the operational envelope that guarantees interfacial bonding between heterogeneous solid materials and preserves wellbore integrity, considering the specific thermo-mechanical properties of the materials involved.

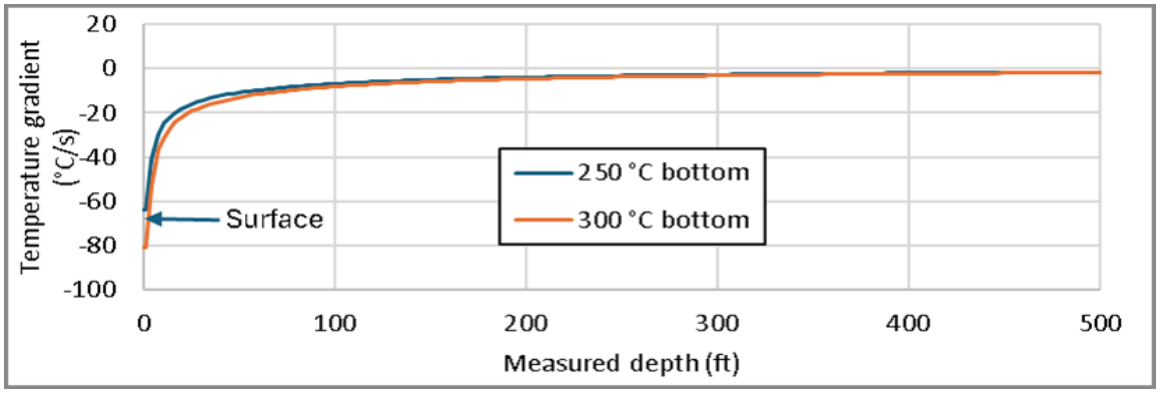

Figure 11: Fluid Maximum Temporal Temperature Gradient during 400 gal/min Injection

In the final stage of wireline operations, after injection is halted, heat transfer is once again governed primarily by natural convection within the wellbore fluid and conduction through the surrounding solids. Figure 12 depicts the temperature distribution along the well depth 24 hrs. after injection shutdown. The profiles show stepwise variations at depths corresponding to changes in casing and cement configurations. Minor steps near the surface are attributed to residual heat from the preceding tempering phase, during which the injected fluid was slightly warmer than ambient conditions. For a 250 °C bottom-hole scenario, the wellhead fluid temperature reaches 74.7 °C after 24 hrs., remaining within the operational limit of 80 °C. Under a 300 °C bottom-hole condition, the overall trend is similar; however, the surface temperature rises to 86.2 °C, slightly exceeding the limit. In such cases, adjustments to tempering flow parameters or a reduction in survey duration may be required.

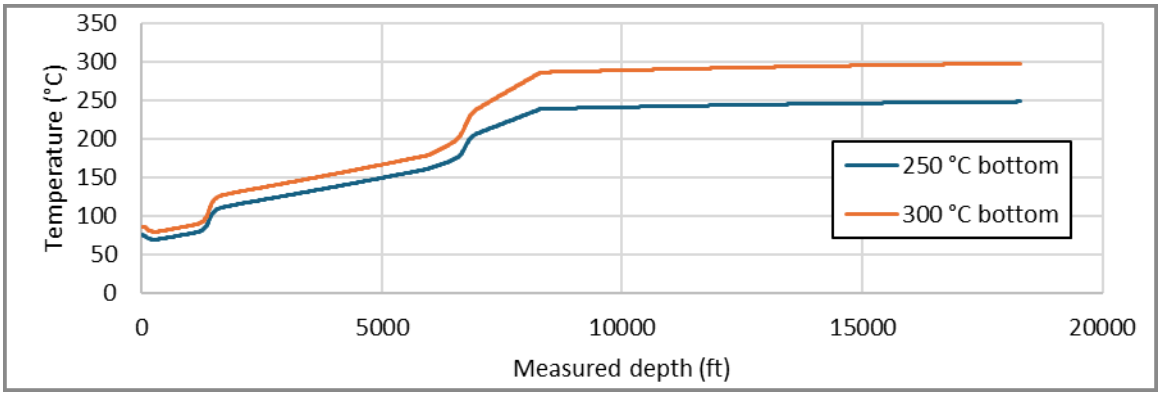

Figure 12: Fluid Temperature Along The Well at 24 Hr. After 400 gal/min Injection Shutdown

Figure 13 illustrates the surface temperature profile during the 24 hrs. shutdown for wireline operations. Notably, the surface temperature stabilizes after approximately 18 hrs. of injection shutdown, indicating thermal equilibrium between the upper fluid layer and the ambient environment. To ensure equipment protection and safe operations, it is essential to account for the wireline operation window or implement alternative measures to effectively reduce surface temperature.

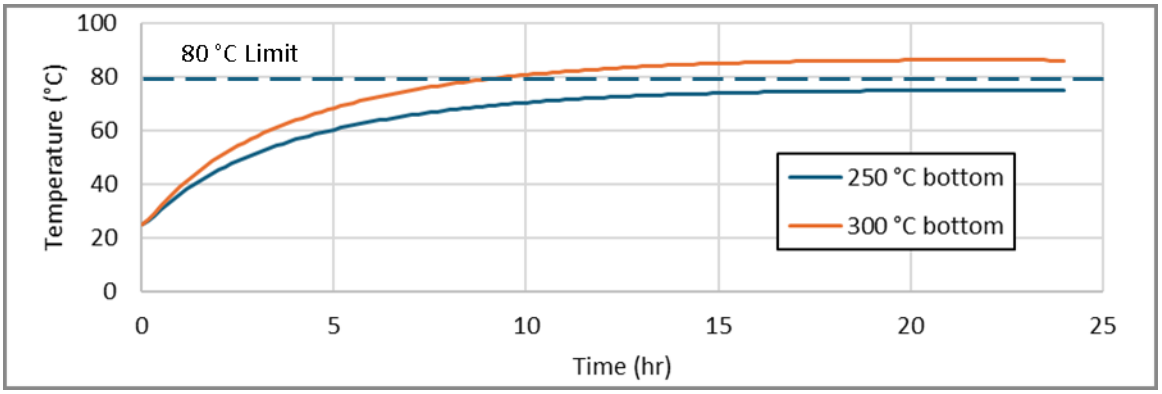

Figure 13: Surface Fluid Temperature During Shut-In and Wireline Operation

The wellhead temperature is influenced by several parameters, including production flow rate, shutdown duration, tempering injection flow rate, and injection temperature. Figure 14 shows the temperature profile along the well depth 24 hrs. after injection shutdown for an injection flow rate of 100 gal/min. Compared to the 400 gal/min case shown in Figure 12, the most noticeable differences occur in the deeper vertical section near the bottom of the well. At the ground surface, however, the temperature difference between the two cases is minimal, i.e. only about 0.5 °C higher for the lower flow rate scenario. This comparison indicates that injection flow rate primarily affects temperature at greater depths rather than near the surface. Consequently, reducing the injection temperature is more effective for controlling wellhead temperature than increasing the flow rate.

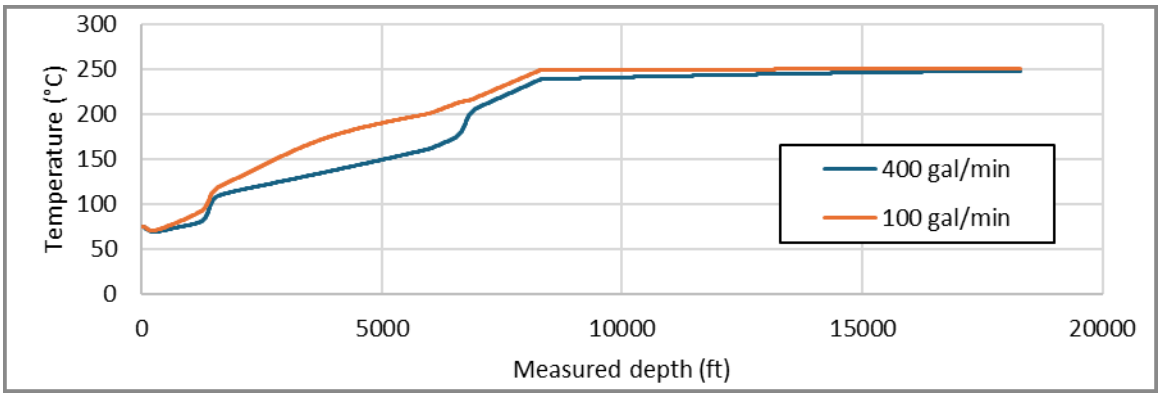

Figure 14: Fluid Temperature at 24 Hr. with 100 gal/min Injection Shutdown for 250 °C Bottom

8. SUMMARY AND CONCLUSIONS

The evolution of temperature during the operational phases—production, shutdown, tempering, and wireline intervention—is governed by complex thermal interactions. Heat conduction within solid components and both forced and natural convection in the wellbore fluid dominate at different stages of operation. To capture these dynamics, a two-dimensional transient wellbore temperature simulation tool was developed and coded in a mathematical programming language. The model solves heat conduction in solid elements, including casing, liner, cement, and surrounding formation, while representing fluid flow using an average velocity approach. Convective heat exchange between the fluid and solids is computed using established correlations for forced convection. The simulation framework was validated against results from a commercial software package. The code shows a speedup of approximately 100 and provides greater flexibility by allowing easy modification of material properties and geometric. This capability simplifies parametric studies and supports design-of-experiment approaches for "what-if" scenarios.

Numerical experiments were performed on an artificial well geometry derived from an existing EGS well, with ambient formation temperatures based on field data. Results indicate that steady-state production outflow temperatures at the wellhead reach 247.9 °C for the 250 °C bottom-hole temperature and 296.7 °C for the 300 °C bottom-hole temperature. The fluid temperature profile exhibits distinct stepwise variations at depths where casing and cement configurations change, driven by differences in radial heat loss and thermal storage associated with varying material thicknesses. The highest temporal temperature gradients occur during the tempering phase, where rapid cooling introduces significant thermal stresses. During the final phase of wireline operation, the surface temperature stabilizes after approximately 18 hrs. of injection shutdown, indicating thermal equilibrium between the upper fluid layer and the ambient environment. For a 250 °C bottom-hole temperature, the wellhead fluid temperature remains below the 80 °C threshold within 24 hrs. of injection shutdown which prevents flashing and steam formation with a 20 °C safety margin. For the 300 °C bottom-hole temperature, the final wellhead temperature slightly exceeds this limit. Additional simulations reveal that increasing tempering flow rate has minimal impact on surface temperature, whereas lowering the injection temperature will be a more effective strategy for thermal control.

The developed simulation approach captures reasonably captures wellbore temperature evolution and transient thermal gradients, providing a practical tool for planning and optimizing temperature management during well conditioning and wireline operations. The final wellhead temperature is influenced by multiple operational parameters. High thermal gradients during tempering can induce thermal stress in casing materials, so controlled ramp-up of injection flow and temperature is recommended to mitigate mechanical risks. Stepwise temperature variations highlight the influence of casing and cement thickness on heat transfer. Wells with bottom-hole temperatures above 300 °C may require longer tempering periods or more aggressive tempering strategies to meet surface temperature limits for wireline safety. For instance, the tempering duration would need to exceed two hours. There might also be a need to extend the wireline operation beyond 24 hrs. Future research should explore these scenarios once detailed formation and temperature profile data become available.

The thermal simulation tool accurately predicts well temperature profiles over time, enabling precise planning of operational phases. Its fast computation supports scenario-based planning, improving intervention efficiency and sensitivity analysis of various control parameters such as injection flow rate, temperature, tempering and wireline survey duration. When integrated with real-time surface temperature measurements, the model can dynamically estimate downhole conditions, allow proactive adjustments and minimize non-productive time. This predictive framework enhances operational safety and reliability by analyzing performance of the well under diverse conditions. It also enables optimization of tempering strategies and supports safe wireline operations in high-temperature environments.

REFERENCES

Allis, R. G., Gwynn, M. L., Hardwick, C. L., Hurlbut, W. W., and Moore, J. N.: Thermal Characteristics of the Roosevelt Hot Springs System, With Focus on the FORGE EGS Site, Milford, Utah, Utah Geological Survey (2019). https://doi.org/10.34191/MP-169-D

Alumbaugh, D., Wilt, M., Nichols, E., Um, E., Pickett, K., Hyodo, M., Arayama, K., and Petrovich, N.: Utah FORGE: LBNL Reports on VEMP Electromagnetic Data Collection and Processing – 2024 [data set], Geothermal Data Repository (2025). https://doi.org/10.15121/2531106

ANSYS, Inc.: Ansys Fluent, Release 2025 R1, Help System, ANSYS, Inc. (2025).

Chaerudin Irwansyah, D., Rifki, G., Agustino, V., Adityatama, D., and Wahyu Wiharlan, H.: Geothermal Well Control Equipment Application for Mining Drilling in Geothermal Environment, Proceedings, New Zealand Geothermal Workshop, Auckland, New Zealand (2021).

Colburn, A. P.: A Method of Correlating Forced Convection Heat Transfer Data and a Comparison With Fluid Friction, International Journal of Heat and Mass Transfer, 7 (1933), 1359–1384.

Dupriest, F. E., and Noynaert, S. F.: Continued Advances in Performance in Geothermal Operations at FORGE Through Limiter-Redesign Drilling Practices, Proceedings, SPE/IADC Drilling Conference and Exhibition (2024). https://doi.org/10.2118/217725-MS

Elshehabi, T., and Alfehaid, M.: Sustainable Geothermal Energy: A Review of Challenges and Opportunities in Deep Wells and Shallow Heat Pumps for Transitioning Professionals, Energies, 18(4) (2025), 811. https://doi.org/10.3390/en18040811

Forterra: Thermalite Aircrete Block Guide: Lightweight, Sustainable and Thermally Efficient [data sheet], Forterra (2021).

Fouad, M. G., and Ibl, N.: Natural Convection Mass Transfer at Vertical Electrodes Under Turbulent Flow Conditions, Electrochimica Acta, 3 (1960), 233–243. https://doi.org/10.1016/0013-4686(60)85007-4

Gwynn, M., Allis, R., Hardwick, C., Jones, C., Nielsen, P., and Hurlbut, W.: Compilation of Rock Properties From FORGE Well 58-32, Milford, Utah, Utah Geological Survey (2019). https://doi.org/10.34191/MP-169-L

Hamm, S. G., Anderson, A., Blankenship, D., Boyd, L. W., Brown, E. A., Frone, Z., et al.: Geothermal Energy R&D: An Overview of the U.S. Department of Energy's Geothermal Technologies Office, Journal of Energy Resources Technology, 143(10) (2021). https://doi.org/10.1115/1.4049581

Incropera, F. P., DeWitt, D. P., Bergman, T. L., and Lavine, A. S.: Fundamentals of Heat and Mass Transfer, 7th ed., John Wiley & Sons, Hoboken, NJ (2011).

Kabeyi, M. J. B.: Geothermal Electricity Generation, Challenges, Opportunities and Recommendations, International Journal of Advances in Scientific Research and Engineering, 5(8) (2019), 53–95. https://doi.org/10.31695/IJASRE.2019.33408

Kirby, S. M., Simmons, S., Inkenbrandt, P. C., and Smith, S.: Groundwater Hydrogeology and Geochemistry of the Utah FORGE Site and Vicinity, in Allis, R. G., and Moore, J. N. (eds.), Geothermal Characteristics of the Roosevelt Hot Springs System and Adjacent FORGE EGS Site, Milford, Utah, Utah Geological Survey Miscellaneous Publication 169-E (2019), 1–21. https://doi.org/10.34191/MP-169-E

Kumar, L., Hossain, M. S., Assad, M. E. H., and Manoo, M. U.: Technological Advancements and Challenges of Geothermal Energy Systems: A Comprehensive Review, Energies, 15(23) (2022), 9058. https://doi.org/10.3390/en15239058

Lellouch, A., Lindsey, N. J., Ellsworth, W. L., and Biondi, B. L.: Low-Magnitude Seismicity With a Downhole Distributed Acoustic Sensing Array—Examples From the FORGE Geothermal Experiment, Journal of Geophysical Research: Solid Earth, 126 (2021). https://doi.org/10.1029/2020JB020462

Lemmon, E. W., Bell, I. H., Huber, M. L., and McLinden, M. O.: NIST Standard Reference Database 23: Reference Fluid Thermodynamic and Transport Properties (REFPROP), Version 10.0, National Institute of Standards and Technology, Gaithersburg, MD (2018). https://doi.org/10.18434/T4/1502528

Martuganova, E., Stiller, M., Norden, B., Henninges, J., and Krawczyk, C. M.: 3D Deep Geothermal Reservoir Imaging With Wireline Distributed Acoustic Sensing in Two Boreholes, Solid Earth, 13 (2022), 1291–1306. https://doi.org/10.5194/se-13-1291-2022

Moya, D., Aldás, C., and Kaparaju, P.: Geothermal Energy: Power Plant Technology and Direct Heat Applications, Renewable and Sustainable Energy Reviews, 94 (2018), 889–901. https://doi.org/10.1016/j.rser.2018.06.047

Naftz, D. L., Millero, F. J., Jones, B. F., et al.: An Equation of State for Hypersaline Water in Great Salt Lake, Utah, USA, Aquatic Geochemistry, 17 (2011), 809–820. https://doi.org/10.1007/s10498-011-9138-z

Saad, Y.: Iterative Methods for Sparse Linear Systems, 2nd ed., SIAM, Philadelphia, PA (2003).

Sausan, S., Hartung, M., Su, J.-C., Schneider, M. B., Wright, A. A., and Horne, R. N.: Updates on the Development of Chloride-Based Wireline Tool for Measuring Feed Zone Inflow in Enhanced Geothermal Systems (EGS) Wells, Proceedings, 49th Workshop on Geothermal Reservoir Engineering, Stanford University, Stanford, CA (2024).

Utah FORGE: End-of-Well Report and Associated Mud Temperature and Wireline Logs for Well 16B(78)-32 [data set], Geothermal Data Repository (2023). https://doi.org/10.15121/1998591

Wolterbeek, T., and Hangx, S.: The Thermal Properties of Set Portland Cements: A Literature Review in the Context of CO_2 Injection Well Integrity, International Journal of Greenhouse Gas Control, 126 (2023), 103909. https://doi.org/10.1016/j.ijggc.2023.10390

Ziagos, J., Phillips, B. R., Boyd, L., Jelacic, A., Stillman, G., and Hass, E.: A Technology Roadmap for Strategic Development of Enhanced Geothermal Systems, Proceedings, 38th Stanford Geothermal Workshop, Stanford University, Stanford, CA (2013). https://doi.org/10.2172/1219933